Suppressing multipacting in a 56 MHz quarter wave resonator

Damayanti Naik and Ilan Ben-Zvi

Collider-Accelerator Department, Brookhaven National Laboratory, Upton New York 11973, USA

(Received 3 April 2009; published 25 May 2010)

We propose using a beam excited 56 MHz radio frequency (rf) niobium quarter wave resonator (QWR) to enhance the luminosity and bunching of the RHIC's (relativistic heavy ion collider's) beam. From experience with similar structures, multipacting is expected but is to be avoided in a storage ring; therefore, we undertook extensive simulations with the MULTIPAC 2.1 2D code. They revealed that multipacting occurs in various bands up to a peak surface electric field of 50 kV/m, and is concentrated mostly above the beam gap and on the outer conductor. To resolve this issue, we introduced a ripple structure into the outer conductor and successfully eliminated multipacting.

DOI: 10.1103/PhysRevSTAB.13.052001 PACS numbers: 52.80.Pi

I. INTRODUCTION

Multipacting, a highly probable occurrence in most evacuated rf structures, is a low field electron avalanche phenomenon caused by resonant electron multiplication from secondary emissions [1,2]. Starting from the walls or inside the cavity, the electrons gain energy from the rf field, as they move along a repetitive path. After hitting the cavity's wall, and, depending on the secondary yield (δ) of the wall's material, they may accumulate in great numbers, thus creating an electron cloud. Subsequently, the cloud absorbs much of the power pumped into the system and prevents the structure from reaching its design field. Furthermore, the impacts of the electrons on the cavity's wall raise its temperature, a serious drawback for superconducting material as it may quench superconductivity. Symmetry in rf structures also increases the strength of multipacting by providing more surface area under the same conditions. Of course, an asymmetric structure offers more potential multipacting locations. Following the detailed design of the 56 MHz quarter wave resonator (QWR) [3], the shape of the cavity is shown in Fig. 1. The cavity is fabricated using high residual resistivity ratio niobium. Initially the cavity did not have the ripple structure on its outer conductor seen in Fig. 1 and it was expected to be susceptible to severe multipacting [2]. Therefore, we carried out simulations of this process in the cavity with a 2D and later with a 3D code. However, the first simulation with the MULTIPAC 2.1 2D code [4] was carried out without a coupler and dampers in the cavity; the present article details our results and offers a method to suppress multipacting there. Our initial simulations with the 3D code verify these findings.

II. SIMULATION CODE FEATURES

The Linux based MULTIPAC 2.1 2D code that represents axial symmetric rf structures is appropriate for modeling the 56 MHz quarter wave cavity without coupler and dampers. Based on the finite element method field solver, the code calculates the time harmonic electromagnetic field. Thereafter, it locates multipacting field levels, aided by data on the secondary yield of the cavity's material. Figure 2 shows the secondary yield from niobium [4,5]. Finally, it details the electrons' resonant trajectories. For this entire operation, and to display the results, the code uses the MATLAB graphical user interface.

The representation of multipacting in the cavity is derived from the secondary electrons generated during the process. The code terms it the enhanced counter function, e_N/C_0, which denotes the ratio of the total number of secondary electrons after N impacts (e_N) to the initial number of electrons (C_0). When the enhanced counter function is greater than 1 for 20 electron impacts, then multipacting is possible (but yet to be verified) at that field level. In our study, we adopted 100 impacts with an enhanced counter function greater than or equal to 10^5 as a statistically significant level.

III. SIMULATION

A. Scanning process

The model of the cavity used to calculate multipacting without coupler and dampers looks as shown in Fig. 3. The peak surface electric and magnetic field in the cavity, respectively, reach 44.19 MV/m and 105.4 mT, for 2.5 MV accelerating voltage across the gap. The maximum electric field is at the gap and the maximum magnetic field at the end of the cavity (Fig. 4). The simulation was carried out for the entire geometry with an initial electron (seed electron) energy of 2 eV, a 5-degree rf phase interval, and a 1 kV/m electric field step. However, the cavity's cross section (the length of the cavity is 154.57 cm with an outer radius of 25 cm) was too large for a single run with the chosen parameters. Therefore, we scanned the full geometry in several runs taking a small portion of the cavity at a time. One such seed-electrons launching zone, 20–40 cm of the cavity is highlighted (in blue) in Fig. 5. The compu-

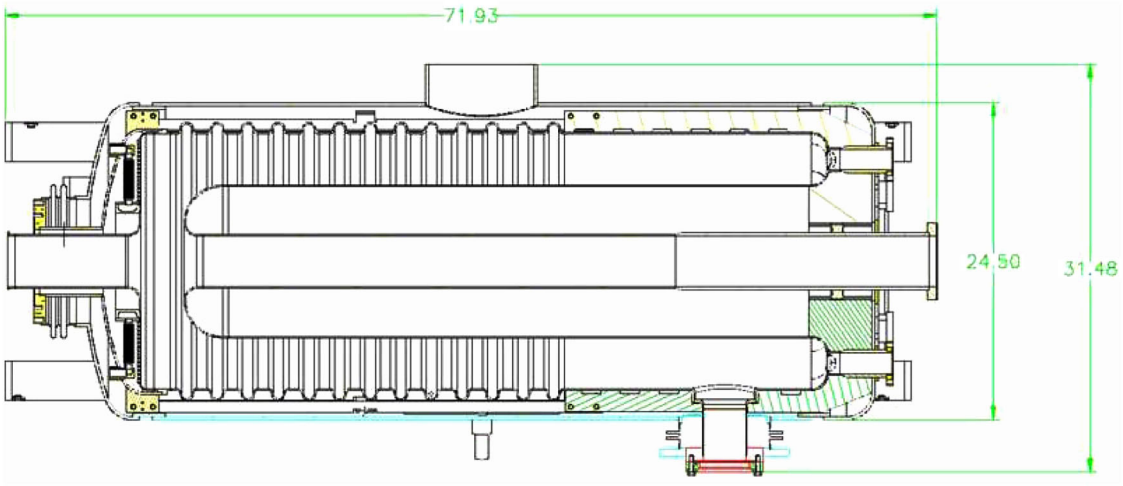

FIG. 1. (Color) The 56 MHz rf quarter wave resonator in its final shape. Dimensions are given in inches. The fundamental damper is at the bottom of the cavity. Other ports are on the right.

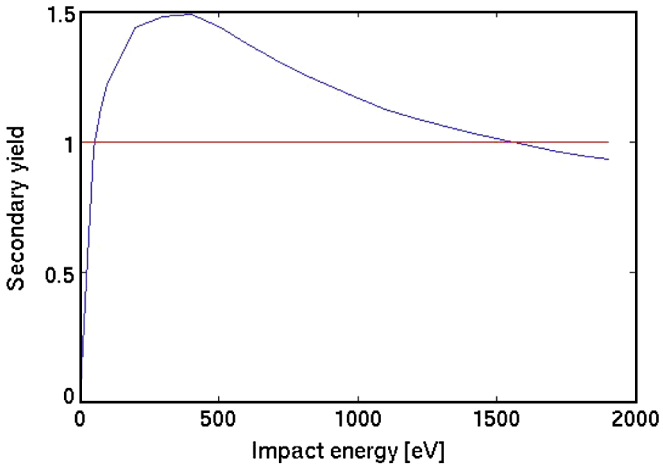

FIG. 2. (Color) Secondary yield for niobium as a function of the electron impact energy in eV.

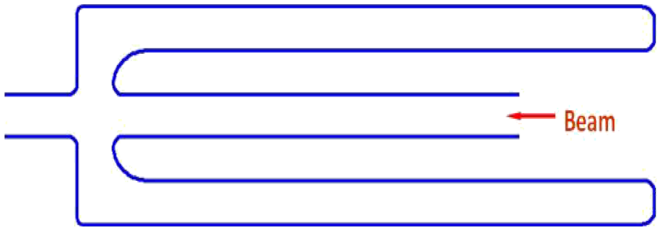

FIG. 3. (Color) Outline of the 56 MHz QWR in two dimensions without the coupler and dampers.

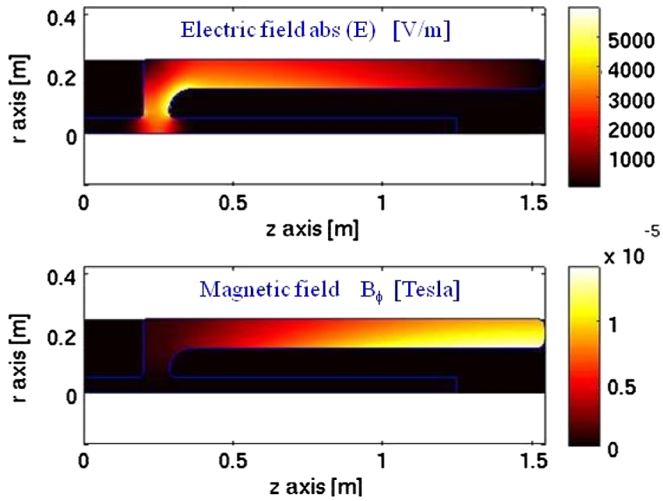

FIG. 4. (Color) Distribution of the electric and magnetic fields in the 56 MHz QWR cavity. This provides a qualitative distribution of the field.

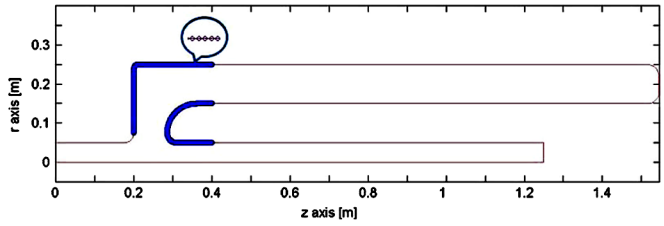

FIG. 5. (Color) Initial electron generation points between 20–40 cm highlighted by blue color.

tation time for the whole cavity was usually 450 hrs on a 32 bit, 2 GB memory Linux working station.

B. Probable multipacting field levels and zones

Simulation data from 100 electron impacts show that multipacting is probable in the cavity. The enhanced counter function plots obtained at different zones of the cavity indicate the likelihood of multipacting at various electric field levels. Some multipacting occurs at the single field whereas some extends to wide bands. The enhanced counter functions for zones 20–40, 40–60, 60–80, and

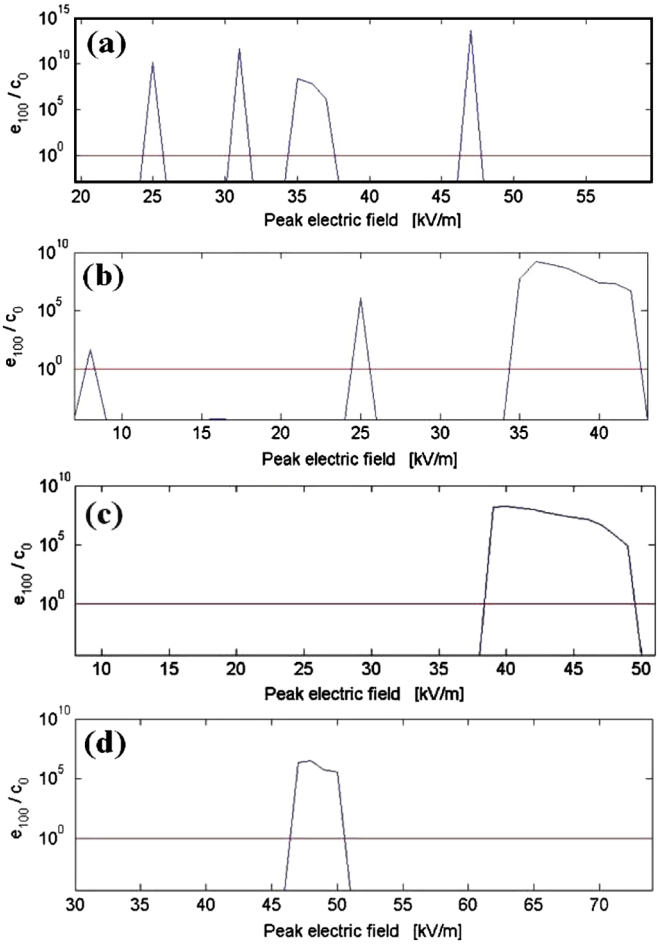

FIG. 6. (Color) (a) Enhanced counter function plot for 20–40 cm of the cavity. Multipacting is probable at peak surface electric field 25, 31, 35–37, and 47 kV/m. (b) Enhanced counter function plot for 40–60 cm of the cavity showing probable multipacting electric field at 25 and 36–44 kV/m. (c) Enhanced counter function plot for 60–80 cm of the cavity. Multipacting is probable in the band of 38–49 kV/m. (d) Enhanced counter function plot for 80–100 cm of the cavity showing multipacting probable band at 47–50 kV/m.

80–100 cm where multipacting is probable (with $e_{100}/C_0 \geq 10^5$) are shown in Figs. 6(a)–6(d). From these plots it is apparent that multipacting levels are found below and at the 50 kV/m peak surface electric field. No multipacting is found above 50 kV/m.

C. Multipacting trajectories

Taking these established probable peak surface electric field levels, electron trajectories are plotted. Both single-point and two-point multipacting are apparent, concentrating mostly above the beam gap and on the outer conductor. Most of the trajectories show a tendency to drift towards the closed end of the cavity.

Starting with the levels shown in Fig. 6(a) for a longitudinal band at 20 to 40 cm of the cavity, the stable electron trajectories are shown in Figs. 7(a)–7(d). At peak surface electric field 25 and 47 kV/m, single-point multipacting [2] is evident on the outer conductor, whereas at 31 kV/m, two-point multipacting [2] is concentrated on the top corner of the cavity. However, at 35 kV/m, the trajectories are of the two-point multipacting variety, moving away from the gap zone and towards the end of the cavity. In one-point multipacting the electrons hit a small area near their point of origin repetitively, once per some number of rf periods. The number of rf periods required by an electron to return to the point of origin is defined as the order of the multipacting. Two-point multipacting occurs when the electron trajectories include two distinct impact points and time between impacts is a half integer, $(2n-1)/2$ multiple of rf periods; here n represents the order of the two-point multipacting.

For the rest of the cavity, the trajectories are shown in Figs. 7(e)–7(j). These trajectories demonstrate that electrons generated from both the inner and the outer conductor can undergo multipacting. However, irrespective of their point of origin, they impact on the outer conductor in single-point multipacting, whereas they strike both the inner and outer conductor in two-point multipacting (viz. an electron generated on the inner conductor at first moves towards the outer conductor and undergoes single-point or two-point multipacting). In all cases, the electrons continue to move towards the closed end of the cavity with the high magnetic field. In this way, the multipacting continues up to 101 cm of the cavity. Here we note that electrons traveling from the outer conductor to the inner conductor do not necessarily follow the same path while reversing their direction; this accounts for the different field strengths the electrons experience during their back and forth oscillations.

In Figs. 7(i) and 7(j), the trajectories of the electrons are not stable and tend to diminish, hence, though they seem as multipacting candidates, they are not multipacting or weak multipacting. Altogether, beyond 101 cm no stable electron trajectories are found and it is therefore considered a multipacting-free zone.

D. Severity over 100 electron impacts

To assess severity, the simulation was continued for more than 100 electron impacts, with some trajectories continuing for 500 and 1000 times or more. Three trajectories which continue up to 1000 times impacts are shown in Figs. 8(a)–8(c). As all the 1000 impacts are not possible to show in the figures, only the last 100 impacts have been detailed out.

IV. COMPARISON OF RESULTS WITH AN OPERATIONAL CAVITY HAVING MULTIPACTING

Our findings, discussed above, reveal that there is multipacting in the cavity. However, to correlate the diagnostics

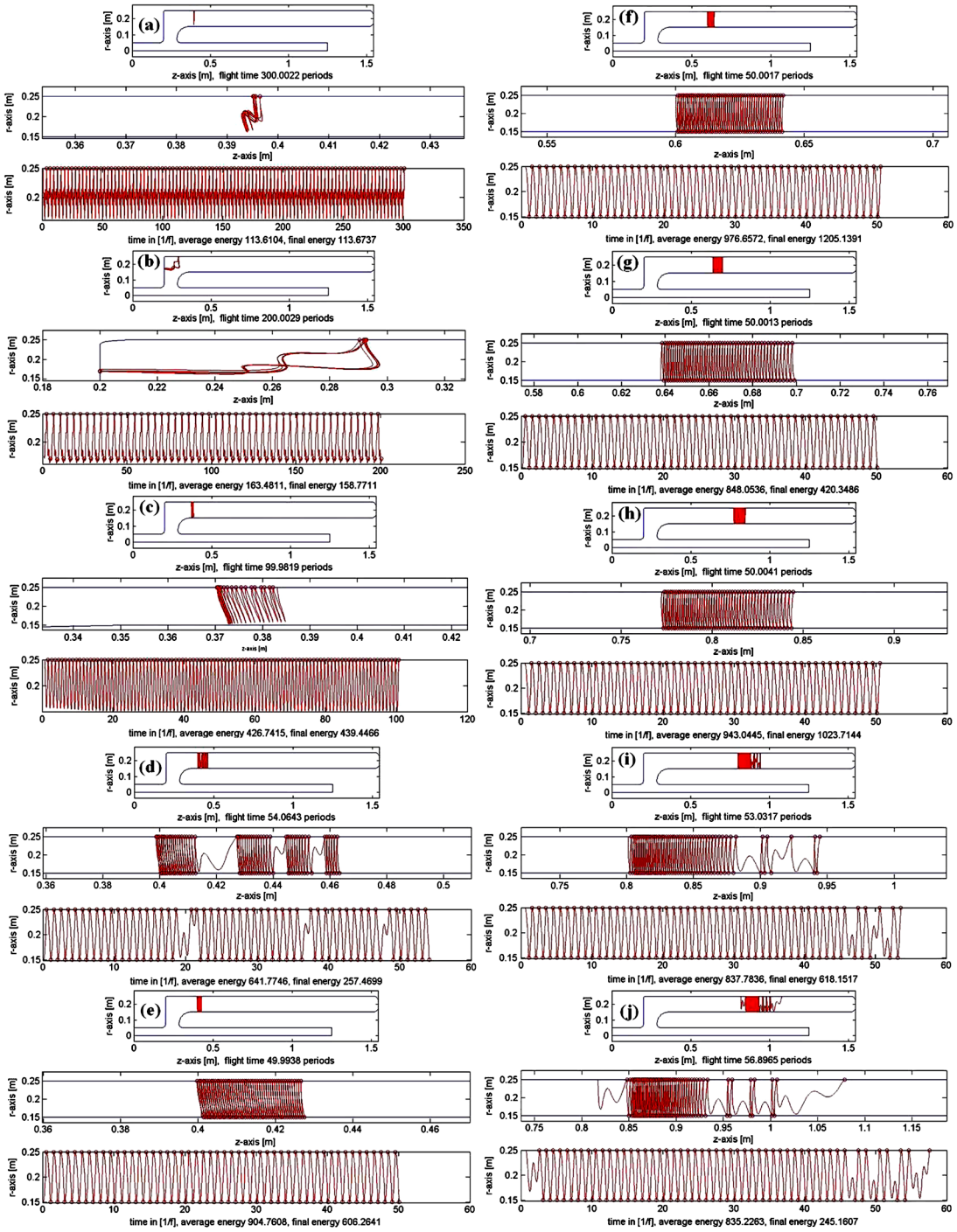

FIG. 7. (Color) (a) The electron's trajectory in third-order single-point multipacting at 25 kV/m. The top figure represents the trajectory of the electron in (r, z) coordinates, the middle one is an expanded plot of a part of the top one, and the bottom plot illustrates the electron's trajectory in the (r, t) coordinates where t is the time in rf periods. The circles indicate the impacts on the walls of the cavity. (b) Electron trajectory in two-point multipacting at 31 kV/m. It is a combination of first and second-order two-point multipacting. (c) The electron's trajectory in first-order single-point multipacting at 47 kV/m. (d) The first-order two-point multipacting electron trajectory at 35 kV/m showing its tendency to move towards the end of the cavity. (e) The first-order two-point multipacting at peak surface electric fields 36 kV/m. (f) The first-order two-point multipacting at peak surface electric fields 40 kV/m. (g) The first-order two-point multipacting at peak surface electric fields 40 kV/m. The stable electron stable trajectories are found right to the multipacting location shown in Fig. 7(f). (h) The first-order two-point multipacting at peak surface electric fields 46 kV/m. (i) The first-order two-point multipacting at peak surface electric fields 46 kV/m. The stable electron stable trajectories are found right to the multipacting location shown in Fig. 7(g). (j) The first-order two-point multipacting at peak surface electric fields 50 kV/m.

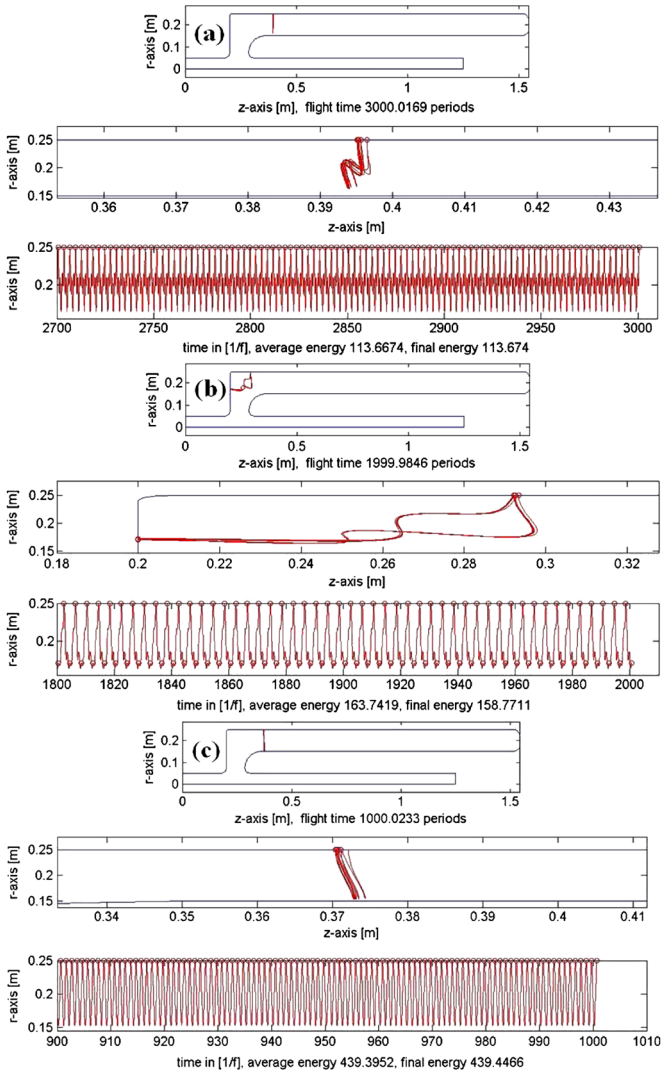

FIG. 8. (Color) (a) One-point multipacting continuing up to 1000 electron impacts at 25 kV/m. In the r axis vs time plot, out of 1000, only the last 100 electron impacts with their stable electron trajectories have been shown. (b) Two-point multipacting continuing up to 1000 electron impacts at 31 kV/m. In the r vs time plot, only the last 100 impacts and their stable electron trajectories are shown. (c) Two-point multipacting continuing up to 1000 electron impacts at 47 kV/m. In the r vs time plot, only the last 100 electron impacts and their stable electron trajectories have been shown.

(such as the enhanced counter function) provided by the multipacting code with a real-life behavior of a cavity, we simulated a cavity wherein multipacting was observed during operation. We chose the 80 MHz quarter wave resonator at LNL (Laboratori Nazionali di Legnaro), Legnaro, Italy [6–9] (Fig. 9), in which multipacting is a known phenomenon affecting the cavity's performance and which is close in frequency and dimensions to our cavity. We were informed that this cavity typically required a few hours to condition its multipacting. This is a manageable situation in a linac, but something that is not desired in

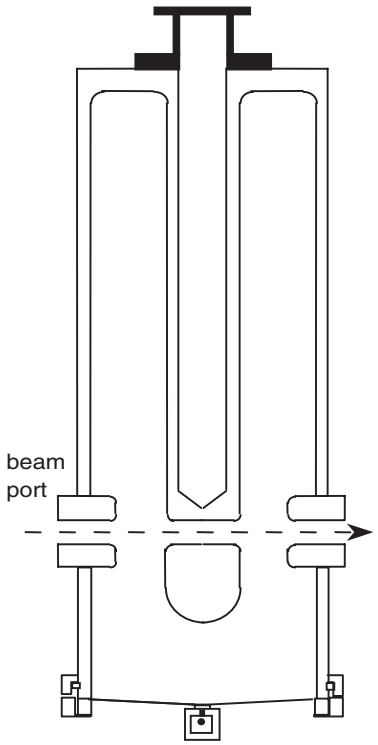

FIG. 9. A mechanical outline of the 80 MHz QWR at LNL, Italy.

a storage ring, which has to cycle every few hours through a new beam load. We made a simple model of the resonator with its beam pipe, and scanned it in multiple runs as was done for our 56 MHz quarter wave resonator. The stable resonant trajectories of the electrons revealed in the coaxial part of the cavity close to the beam pipe at peak surface electric field (E_p) 65 and 71 kV/m which corresponds to accelerating electric field (E_a) of 13 and 14 kV/m as $E_p/E_a = 4.9$ for this cavity. The trajectories are constant for more than 100 electron impacts (we continued the calculation up to 500 impacts), generating an intense electron cloud; this finding agrees with the multipacting observed between 10–20 kV/m accelerating electric field during the first few operational hours of the cavity. The electron trajectories for 500 impacts at 71 kV/m have been shown in Fig. 10. The simulated electron trajectories and electron intensities in the 80 MHz QWR look similar to what we found in our 56 MHz QWR, and established an interpretation of the multipacting code results.

V. SUPPRESSION

A cavity susceptible to strong multipacting cannot operate reliably in a storage ring. Here we note that the multipacting issues in a storage ring cavity are different than in a linac for a few reasons. First, the storage ring is repeatedly cycled and the cavity must be turned off periodically; in RHIC every few hours. Conditioning the cavity

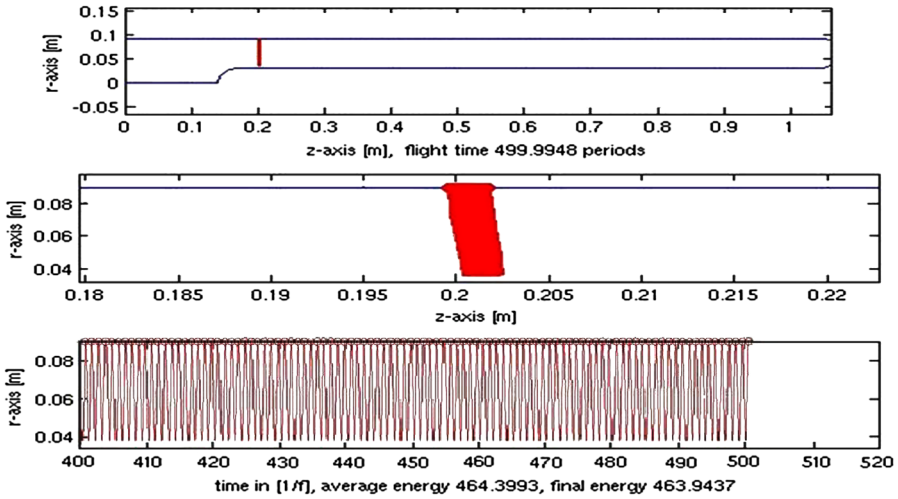

FIG. 10. (Color) The first-order one-point multipacting at peak surface electric field 71 kV/m in the 80 MHz QWR. The total number of electron impacts is 500, out of which only the last 100 impacts have been shown.

for every beam cycle is prohibitive in operational time. Second, the cavity is designed to be beam driven and thus the field can be changed only very slowly, by running a mechanical tuner. Therefore, even once the cavity is conditioned to high field, there is need to repeatedly drive it slowly through multipacting regions. Finally, with the storage ring's current in the cavity, multipacting would destabilize the beam through noise and would require dumping the beam, a very undesirable situation. Hence, we must suppress the multipacting phenomenon in the 56 MHz QWR. We reasoned, the most effective way to do so is by breaking the electron's stable resonant trajectory, thereby preventing its further multiplication, irrespective of the cleanness of the niobium surface. While there are several approaches to control multipacting from outside the superconducting cavity, for example, by applying a DC field [2], these methods are not practical. As a useful alternative, we considered modifying the structure of the cavity, and hence, we undertook simulations with various structures, such as using an outer conductor with a bigger radius (Fig. 11), and ones with ripples pointing downwards (Fig. 12) or upwards. Among them, the latter approach, i.e., incorporating ripples pointing upwards, was the most promising (Fig. 13).

Cavity with optimized ripple

To reduce manufacturing costs, the ripples were optimized to a customary depth and width; we ensured they are sufficiently separated. In addition, adequate space must be left for the coupler and dampers at the end of the cavity. We considered ripples with depths up to 2 cm, and widths from 1–3 cm, with the maximum possible separation between them. Simulations revealed that with 1 cm deep ripples, the electrons maintain resonant trajectories in the ripple zone,

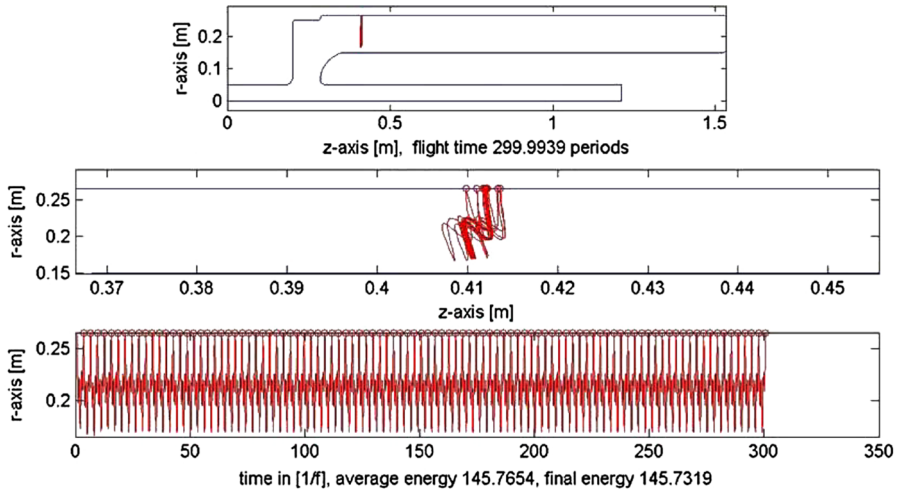

FIG. 11. (Color) Multipacting in the outer conductor with a bigger radius (>25 cm).

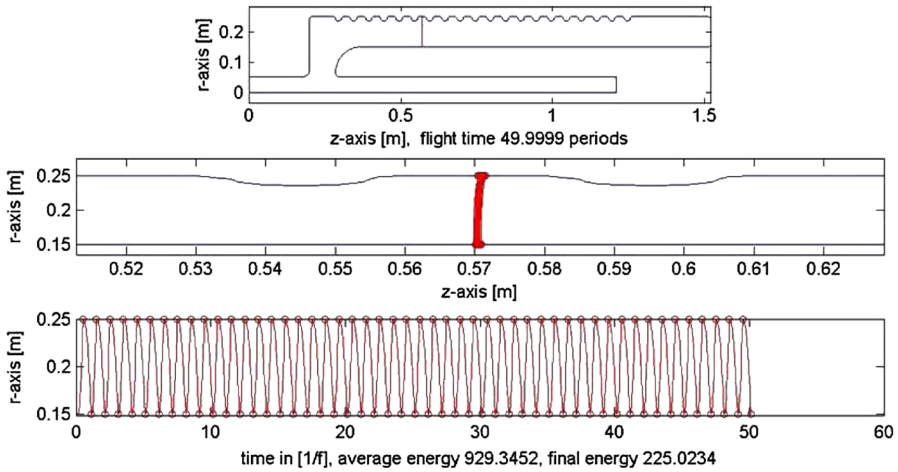

FIG. 12. (Color) Multipacting in the cavity when ripples point downwards.

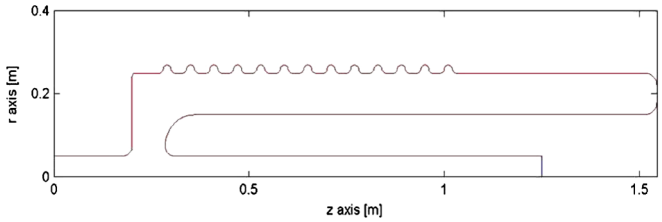

FIG. 13. (Color) Ripples pointing upwards.

moving further and further while multiplying. Mechanical engineering constraints on the material's curvature also prohibit shallow ripples. However, 2 cm deep ripples satisfy the requirements. The ripple's width also is critical. A 1 cm wide ripple is unsatisfactory as electrons can emerge from it, whereas they undergo resonant oscillation inside a 3 cm ripple, and are trapped there (Fig. 14). We chose to avoid using 3 cm wide ripples, even though the energy of the electrons is only a few eV less ($\delta > 1$ at 55 eV) to be on the conservative side. The 2 cm wide ripples are a good choice. Likewise, it is essential to determine the gap between the ripples. The stable trajectory of the electron is favored by having gaps over 2 cm. Figure 15 depicts the stable electron trajectories for a gap of 4 cm between the ripples; in contrast, Fig. 16 illustrates the breaks in electron trajectories with 2 cm gap, even for 20 impacts.

Finally, we demonstrated that ripples, 2 cm deep, 2 cm wide, with an intervening 2 cm gap completely suppressed multipacting in the cavity.

The ripples are made in 27–102 cm of the cavity, because ripples before 27 cm favors two-point multipacting across the corner, whereas the electric and magnetic field in the straight section at $z > 102$ does not support multipacting. This gives us enough space to place coupler and damper at the end of the cavity.

VI. 3D CODE SUPPORTS RESULTS FROM 2D

Though the results from the 2D code are sound, we carried out a simulation with a 3D code able to handle

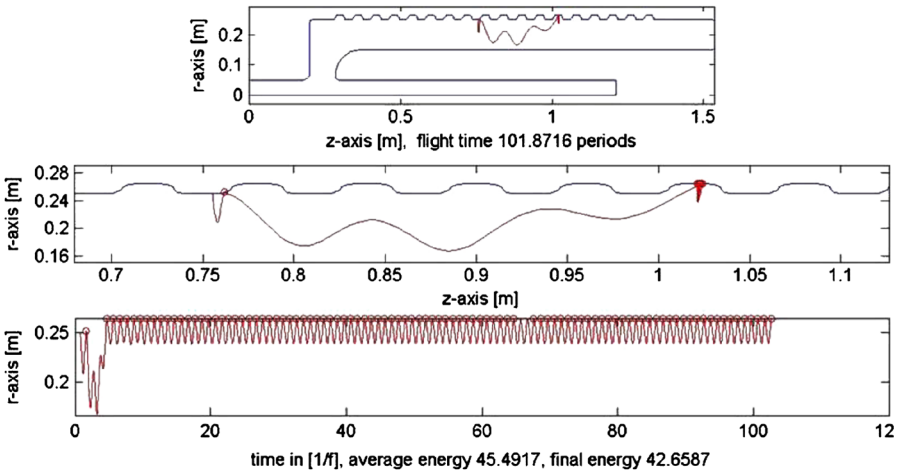

FIG. 14. (Color) Stable trajectories of electrons inside a 3 cm wide ripple.

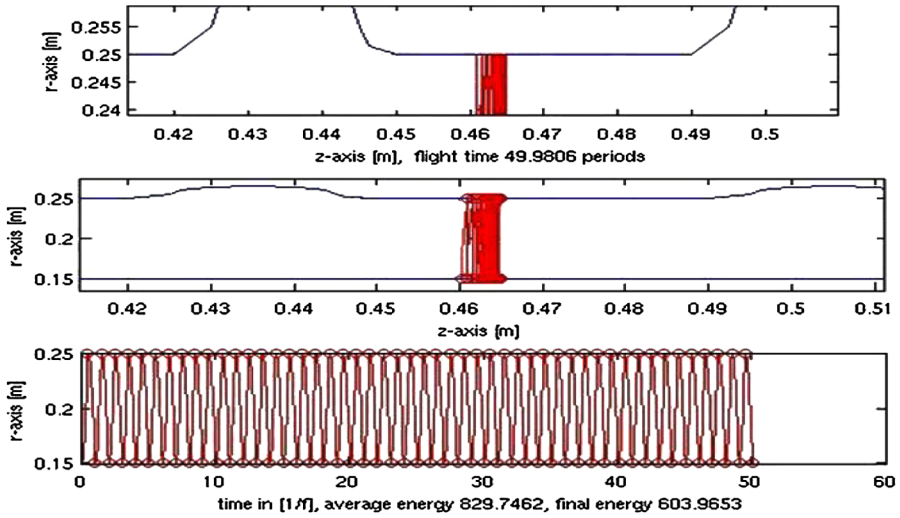

FIG. 15. (Color) Multipacting trajectory with a 4 cm gap between the ripples.

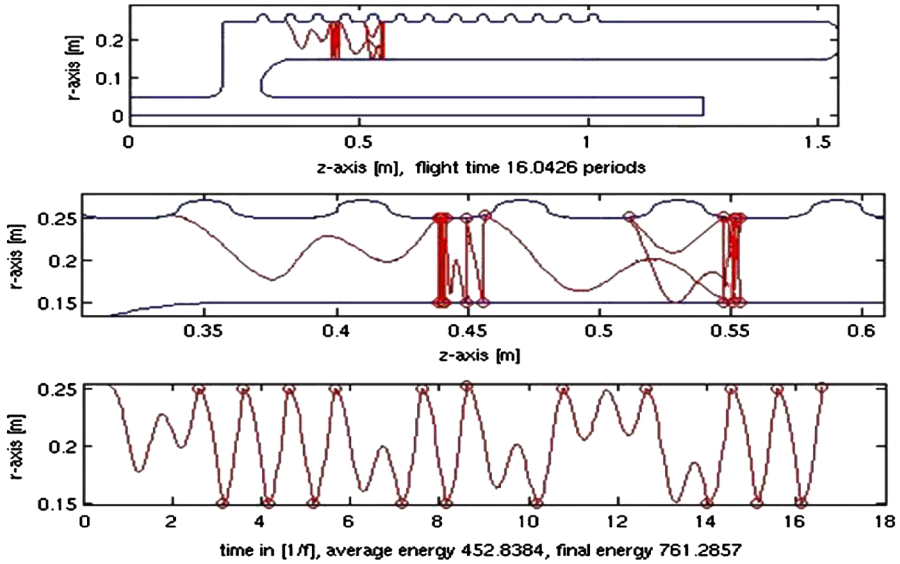

FIG. 16. (Color) Discontinuities in the resonant electron's trajectory with a gap of 2 cm between ripples, even for only 20 impacts.

asymmetry in the geometry due to coupler and dampers. We used the SLAC (Stanford Linear Accelerator Center) electromagnetic parallel 3D code [10,11], comprising a group of programs, out of which OMEGA3P resolves the electromagnetic field in a rf cavity, and TRACK3P searches for multipacting. The code accepts the cavity modeled and meshed in CUBIT 11 [12]. We note that in this paper we discuss only a cylindrically symmetry cavity with no coupler and dampers.

The electromagnetic parallel code runs in NORIC (SLAC's Unix machine) and in NERSC's (National Energy Research Scientific Computing Center's) [13] parallel computing system using distributed memory. The TRACK3P utilizes the NORIC computing tool, whereas OMEGA3P is loaded in BASSI [14] of NERSC's computing system. The computation time for the 56 MHz QWR cavity in 3D using the massively parallel computer was 175 hours.

We found out that the 3D simulation also indicated the existence of multipacting in the cavity, with very little difference from the 2D code. For the cavity lacking ripples (no corrugations) multipacting occurs up to peak surface electric field 45 kV/m and covers up to 87 cm of the cavity. For the corrugated cavity, multipacting was completely suppressed, though a few (3) electrons at 91.5 cm of the cavity are able to make up to 100 impacts. Note that as the 3D code is still under development, we took the 3D results as an additional tool to support our 2D results.

Thus, simulation with both 2D and 3D codes indicate multipacting in the cavity and ability of the corrugation to suppress multipacting.

VII. EVALUATION OF MULTIPACTING SUPPRESSION USING AN ENHANCED SECONDARY YIELD

To account for possible stronger multipacting due to any type of poor surface of the niobium, we tested the performance of the ripple-patterned cavity with double the secondary yield of electrons with 2D code. The region of δ larger than 1 in this simulation was extended and widened from 54–1554 to 25–4105 eV. No multipacting level was evident, even under this large secondary emission coefficient. This finding confirms the robustness of the rippled cavity against multipacting. Therefore, we adopted the pattern of ripples 2 cm deep, 2 cm wide separated by a 2 cm gap for designing the cavity.

Finally, we highlight the difference between the ripples introduced in our quarter wave resonator to eliminate multipacting, and earlier grooving techniques [15]. The latter aims at disturbing the electrons' trajectories near the grooves. In contrast, the ripple structure breaks the multipacting-resonance condition along the quarter wave resonator. Another advantage of the gentle ripples is evident in the ease of chemical cleaning and high-pressure rinsing of the cavity.

VIII. CONCLUSION

The 2D simulations, and cross-check with the 3D code, revealed multipacting in the conventionally shaped 56 MHz QWR. The strength of the multipacting, as given by the program, was compared to a cavity of similar shape with operational experience. We show that we can eliminate multipacting in this cavity by structurally modifying its walls with ripples. However, as normally the cavity is equipped with a coupler and dampers, we are carrying out a complete simulation with the 3D code to confirm a multipacting-free cavity. The cavity's shape, determined by the 2D code, was approved for fabrication.

ACKNOWLEDGMENTS

We thank Anna Marie Porcellato for sharing her experience with multipacting while operating the 80 MHz quarter wave resonator at LNL, Italy. We appreciate the guidance of Lixin Ge, Lie-Quan Lee, Greg Schussman, Cho-Kuen Ng, Zenghai Li, and Kwok Ko of SLAC Advanced Computation Department in carrying out our simulations with 3D electromagnetic parallel code. This work has been supported by the U.S. Department of Energy.

[1] A. J. Hatch *et al.*, Phys. Rev. **112**, 681 (1958).
[2] H. Padamsee, J. Knobloch, and T. Hays, *RF Superconductivity for Accelerators* (Wiley, New York, 1998).
[3] I. Ben-Zvi, BNL Collider-Accelerator Department Accelerator Report C-A/AP/337, http://www.bnl.gov/cad/ecooling/papers.asp.
[4] P. Ylä-Oijala *et al.*, *MultiPac 2.1—Multipacting Simulation Toolbox with 2D FEM Field Solver and MATLAB Graphical User Interface*, User's manual (Rolf Nevanlinna Institute, Helsinki, 2001).
[5] R. Calder *et al.*, Nucl. Instrum. Methods Phys. Res., Sect. B **13**, 631 (1986).
[6] A. Facco *et al.*, Nucl. Instrum. Methods Phys. Res., Sect. A **328**, 275 (1993).
[7] A. M. Porcellato *et al.*, in *Proceedings of the 12th International Workshop on RF Superconductivity* (Cornell University, Ithaca, New York, 2005).
[8] S. Stark *et al.*, LNL Annual Report-2007, p. 148.
[9] http://epaper.kek.jp/e96/PAPERS/WEPL/WEP033L.PDF.
[10] http://www-group.slac.stanford.edu/acd/Codes.html.
[11] Z. Li *et al.*, in *Proceedings of the 2007 Particle Accelerator Conference, Albuquerque, New Mexico* (IEEE, Albuquerque, New Mexico, 2007), p. 889.
[12] http://cubit.sandia.gov/.
[13] http://www.nersc.gov.
[14] http://www.nersc.gov/nusers/systems/bassi/.
[15] H. Padamsee *et al.*, IEEE Trans. Magn. **17**, 947 (1981).